Research Square

Preprints are preliminary reports that have not undergone peer review.
They should not be considered conclusive, used to inform clinical practice,
or referenced by the media as validated information.

Physical Artificial Intelligence-Driven Robotic Platform for Autonomous Intravascular Injection and Pharmacokinetic Applications

Kyeong-Ryoon Lee

kyeongrlee@kribb.re.kr

Korea Research Institute of Bioscience and Biotechnology (KRIBB)

Yoon-Jee Chae

Konyang University

Jaeyoung Lee

University of Science and Technology(UST)

Hyeon-Cheol Jeong

Korea Research Institute of Bioscience and Biotechnology (KRIBB)

Ryeo-Won Kim

Research Institute of Intelligence of Biotech PLASBIO Inc.

Hui-Jeong Gwon

Korea Atomic Energy Research Institute (KAERI)

Ki-Suk Kim

Korea Institute of Toxicology (KIT)

Ki-Hwan Nam

Korea Basic Science Institute (KBSI)

Sung Gurl Park

Research Institute of Intelligence of Biotech PLASBIO Inc.

Article

Keywords:

Posted Date: November 25th, 2026

DOI: https://doi.org/10.21203/rs.3.rs-11466051/v1

License: This work is licensed under a Creative Commons Attribution 4.0 International License.
Read Full License

Additional Declarations: Yes there is potential Competing Interest. S.G.P. and R.-W.K. are employees of PLASBIO Inc., which developed and manufactures the robotic injection system (AIIS) evaluated in this study. The other authors declare no competing interests.

Physical Artificial Intelligence-Driven Robotic Platform for Autonomous Intravascular Injection and Pharmacokinetic Applications

Yoon-Jee Chae[1,†], Jaeyoung Lee[2,3,†], Hyeon-Cheol Jeong[3,4,5], Ryeo-Won Kim[6], Hui-Jeong Gwon[7], Ki-Suk Kim[8,9], Ki-Hwan Nam[10], Sung Gurl Park[6,*] and Kyeong-Ryoon Lee[2,3,4,5,*]

[1] Department of Pharmacology, College of Medicine, Konyang University, Daejeon 35365, Republic of Korea

[2] Department of Bioengineering, University of Science and Technology, Daejeon 34113, Republic of Korea

[3] Advanced Alternative Testing Team, Korea Research Institute of Bioscience and Biotechnology, Cheongju, 28116, Republic of Korea

[4] Laboratory Animal Resource & Research Center, Korea Research Institute of Bioscience and Biotechnology, Cheongju 28116, Republic of Korea

[5] Korea Preclinical Evaluation Center, Korea Research Institute of Bioscience and Biotechnology, Daejeon, 34141, Republic of Korea

[6] Research Institute of Intelligence of Biotech PLASBIO Inc., Jeonju 54852 Republic of Korea.

[7]Advanced Radiation Technology Institute, Korea Atomic Energy Research Institute, Jeongeup 56212, Republic of Korea.

[8] Division of Advanced Predictive Research, Korea Institute of Toxicology, Daejeon 34114, Republic of Korea.

[9] Human and Environmental Toxicology, University of Science and Technology, Daejeon 34113, Republic of Korea.

[10] Division of Scientific Equipment Development, Korea Basic Science Institute, Daejeon 34133, Republic of Korea

†These authors contributed equally to this work.

***Corresponding authors:**

Sung Gurl Park

Research Institute of Intelligence of Biotech PLASBIO Inc., Jeonju 54852, Republic of Korea

Tel: +82-63-212-7052

E-mail: plasboss@plasbt.com

Kyeong-Ryoon Lee, Ph.D.

Advanced Alternative Testing Team, Korea Research Institute of Bioscience and Biotechnology, Cheongju, 28116, Republic of Korea

Tel: +82-43-240-6525

E-mail: kyeongrlee@kribb.re.kr

Abstract

Tail vein intravenous injection in mice is a fundamental procedure used in preclinical, pharmacokinetic, and pharmacological studies; however, it remains highly operator-dependent and susceptible to variability and extravasation. To address these limitations, we developed a physical artificial intelligence (AI)-based automated intravascular injection system (AIIS) that integrated deep-learning-based vision, robotic actuation, optimized optical illumination, and real-time pressure feedback within a closed-loop control framework. The AIIS employed a DeepLabv3+ convolutional neural network for real-time tail vein segmentation under wavelength-optimized green light-emitting diode illumination (525–550 nm), enabling robust vein recognition across mouse strains with differing tail pigmentation. Vision-based alignment, robotic micro adjustments, and pressure-based confirmation of venous entry facilitated autonomous and precise needle insertion and achieved high injection success rates of 90%–96% with submillimeter spatial precision. To evaluate the suitability of AIIS for quantitative drug studies, caffeine was administered intravenously at doses of 1, 5, and 10 mg/kg, and the plasma concentrations were analyzed using liquid chromatography-tandem mass spectrometry. The resulting pharmacokinetic profiles declined monoexponentially with short elimination half-lives (0.52–0.59 h) and exhibited dose-dependent changes in systemic exposure, consistent with established mouse caffeine pharmacokinetics. Overall, this study demonstrates that AIIS enables precise, reproducible, and ethically refined intravenous administration in mice and represents a practical application of physical AI for standardized in vivo preclinical research.

Introduction

Over the past decades, advances in high-throughput screening, omics technologies, and automated analytical platforms have markedly expanded the scale and complexity of preclinical biomedical research[1,2,3]. These developments have enabled the rapid generation of large datasets across pharmacology, toxicology, and systems biology, thereby accelerating drug discovery and development[4,5].Despite these technological advances, several experimental procedures in pharmacokinetics (PK) and preclinical pharmacology remain dependent on manual operation. Core experimental steps such as compound administration and sample handling are frequently performed by trained personnel, introducing operator-dependent variability that compromises reproducibility and quantitative reliability. This contributes to broader reproducibility challenges in preclinical research, where variability in experimental execution leads to inconsistencies across studies and laboratories.

Among these procedures, intravenous (IV) administration in small animal models is typically utilized for evaluating systemic drug exposure and PK behavior. In particular, tail vein injection in mice is widely used because of its accessibility and suitability for repeated dosing; however, it remains technically demanding owing to the small diameter (approximately 0.3 mm) and fragility of the lateral tail veins[6,7]. Successful administration requires precise needle alignment and controlled insertion depth, and even minor deviations can result in partial or failed intravascular delivery that leads to extravasation, wherein the injected solution leaks into the surrounding tissues rather than entering the systemic circulation. Tail vein injections are associated with significant failure rates and procedural difficulties, particularly for inexperienced operators or under suboptimal conditions[8]. Importantly, extravasation occurs in preclinical settings, particularly under inexperienced operators or suboptimal techniques, causing significant variability in dosing accuracy. These events significantly alter the effective delivered dose, underestimate systemic exposure, distort concentration-time profiles, and increase variability in PK parameters.

From a PK perspective, such variability is particularly problematic because IV administration is utilized to determine fundamental PK parameters, including clearance (CL), volume

of distribution (Vd), and absolute bioavailability. Therefore, the propagation of errors in dosing or incomplete intravascular delivery through downstream analyses can affect model fitting, parameter estimation, and interpretation of drug disposition. Despite its importance, injection-related variability is often not explicitly accounted for in PK studies, and its contribution to experimental noise remains underrecognized. Consequently, improving the precision and reproducibility of IV administration is a critical yet unmet need in preclinical drug evaluation.

Various automation strategies have been explored to address operator-dependent variability, including image-guided robotic systems and vision-assisted vascular access devices. The feasibility of automating tail vein injections using computer vision and robotic positioning, such as stereo vision or image-based vein detection to guide needle insertion and improve the targeting accuracy, has been successfully demonstrated with under controlled experimental conditions[6,7,9]. However, because these systems typically operate in an open-loop or semiautomated manner and rely primarily on visual information without incorporating direct physiological feedback[10], they exhibit limited ability for successful intravascular access or adaptation to biological variability across individual animals. Factors such as differences in tail pigmentation, vessel geometry, tissue compliance, and local hemodynamics, which affect injection outcomes, are not fully captured by vision-based systems alone. Thus, conventional automation approaches designed for static, well-controlled environments are typically inapplicable to dynamic biological systems.

Recent advances in artificial intelligence (AI) and robotics have resulted in closed-loop experimental platforms that integrate perception, decision-making, and actuation. In in vitro settings, such approaches have been successfully implemented in self-driving laboratories, where AI algorithms iteratively design experiments, analyze results, and refine conditions to optimize outcomes[11,12]. These systems have considerably improved efficiency, reproducibility, and scalability; however, their extension to in vivo experiments in inherently complex and variable living organisms is limited. Biological systems exhibit dynamic physiological states, interindividual variability, and context-dependent responses that cannot be fully captured by static models or predefined control rules,

and effective automation requires continuous sensing of biological signals and adaptive control strategies that respond to real-time feedback.

The emerging concept of physical artificial intelligence (physical AI) provides a promising paradigm for bridging the gap between digital intelligence and real-world biological interaction. Physical AI systems integrate perception, cognition, and physical actuation within a unified feedback loop, enabling machines to continuously sense environmental states, make context-aware decisions, and execute precise actions[13]. Unlike conventional automation that follows predefined routines, physical AI emphasizes adaptive interactions with dynamic environments through real-time feedback[14], which supports biomedical applications that require high precision and responsiveness to physiological signals, such as microsurgery, robotic manipulation, and in vivo experimental procedures[15].

In this study, we developed a physical AI-based automated intravascular injection system (AIIS) that integrates deep learning-based vision, robotic manipulation, and real-time pressure feedback within a fully closed-loop control framework. The system combines visual recognition of the tail vein with physiological confirmation of intravascular access through pressure sensing, enabling continuous perception–decision–action integration during the injection process. Unlike conventional image-guided systems, the AIIS adaptively responds to biological variability by incorporating both visual and physiological information into its control logic. To evaluate its practical utility in preclinical pharmacology, we applied this system to intravenously administer caffeine to mice and assessed the resulting PK profiles. This study links automated injection with quantitative PK evaluation to demonstrate the feasibility of physical AI in in vivo experimentation and for reducing operator-dependent variability and improving the reliability of preclinical drug studies.

RESULTS

Tail Vein Recognition using Vision Machine Learning

The mouse tail vein was automatically identified using a vision-based machine learning model integrated into the AIIS platform. As shown in Fig. 1, the system employed a DeepLabv3+ CNN architecture optimized for high-precision image segmentation. Within the AIIS GUI, the trained model generated a real-time overlay of the recognized vein (red line) and needle trajectory (green line). During the injection process, the system continuously monitored the relative positions of these two features and maintained precise targeting by automatically adjusting the alignment of the robotic arm. The average detection latency per frame was less than 0.15 s, which enabled real-time response to subtle positional shifts caused by tail movement or lighting fluctuations. The deep learning model was trained on a dataset comprising 2,000 labeled tail images obtained from BALB/c, C57BL/6, and ICR mice, which differed in tail pigmentation and vascular contrast. Despite these variations, the trained DeepLabv3+ model achieved a mean intersection-over-union (mIoU) accuracy of 93.2% for vein segmentation, performing robustly under diverse optical conditions. The model maintained consistent detection accuracy without requiring manual calibration between animals, which effectively reduced operator dependence and experimental variability. Thus, vision-based deep learning reliably identifies and tracks mouse tail veins in real time, forming the perceptual foundation of physical AI-based AIIS systems.

Optimization of LED Illumination for Tail Vein Visibility

The effect of the LED illumination wavelength on tail vein contrast was systematically evaluated to enhance vein visibility and ensure reliable recognition by the vision-based AI model. Representative images and intensity profiles of the tail veins of BALB/c, C57BL/6, and ICR mice under differently colored LED lights are presented in Fig. 2. In all strains, illumination with green LED light (wavelength: 525–550 nm) produces the highest contrast between the lateral vein and surrounding

tissue, as evidenced by the largest change in gray-scale intensity (ΔGray value) along the pixel profile. Under natural light or other illumination conditions (blue: 460–470 nm, yellow: 588–596 nm, red: 620–630 nm, white: 7000–8000 K), the boundary between the vein and adjacent tissue appears less distinct, particularly in the pigmented C57BL/6 mice, where melanin reduces light penetration. Quantitative analysis of gray-scale intensity value differences confirmed that green LED illumination provided a clearer and more stable vein signal, improving the image segmentation accuracy for both mouse strains. The custom-designed LED module and tail restrainer (Fig. 2d) ensured consistent illumination geometry and minimized positional artifacts during imaging. These results demonstrated that wavelength-optimized green LED lighting significantly enhanced tail vein detectability, thereby increasing the robustness of the AI-based recognition algorithm and enhancing the overall stability of the automated injection process.

Real-Time Pressure Sensor Monitoring

To confirm accurate intravascular insertion and monitor the injection dynamics, an integrated pressure sensor module was used to continuously record real-time pressure values. The representative pressure-time profiles (Fig. 3) exhibited distinct signal patterns corresponding to the key operational stages of the AIIS. The injection process was characterized by four identifiable points in the pressure profile, namely, Points 1, 2, 3, and 4, which corresponded to the robot stopping point before needle insertion, maximum pressure value immediately after reagent injection, minimum pressure value observed just before the end of the injection as the system prepared to return, and stabilized pressure level after the robot returned to its initial detection position, respectively. During successful intravascular injections, the pressure curve rapidly increased above 4–7 mmHg upon vessel entry (transition from the extravascular to intravascular phase), followed by a transient peak during reagent infusion (Point 2) and a gradual decline toward baseline (Point 4). In contrast, extravascular insertions produced irregular and lower-magnitude pressure fluctuations (< 3 mmHg), indicating the absence of venous access.

To evaluate biological variability, the pressure values were compared across three mouse strains (C57BL/6, BALB/c, and ICR). All strains exhibited the same qualitative pressure pattern: an initial increase, a stable plateau during injection, and recovery to baseline, demonstrating that the AIIS algorithm effectively adapted to inter-strain physiological differences. In addition, a comparison of the sensor data before and after algorithm optimization revealed improved stability and reduced noise amplitudes (Fig. 3) that improved the detection accuracy of the intravascular transition point and minimized false positives in vein identification. Collectively, these findings validate the reliability of pressure-based feedback as a quantitative marker of venous entry and confirm that the AIIS closed-loop control successfully maintains real-time adaptability during injection.

Spatial Precision and Reproducibility of Robotic Motion

Three-dimensional visualization of the recorded motion trajectories demonstrated a highly consistent reproduction of the programmed injection workflow across repeated trials (Fig. 4). The positional deviations of the robotic end effector remained within ±0.2 mm along all three spatial axes (X, Y, and Z). The smooth and repeatable trajectories throughout all the stages of the injection process indicated stable robotic execution under closed-loop control. This level of spatial precision confirms the robustness of the AIIS motion control algorithm and its effective synchronization with the vision-based targeting and pressure feedback systems. Collectively, these results demonstrate that the robotic subsystem provides reliable and consistent intravascular access during automated injection.

Visual Performance Evaluation

The performance of the physical AI-based AIIS was evaluated by visually comparing the injection success rates among BALB/c (albino), C57BL/6 (pigmented), and ICR mice, which differed in tail skin color and vascular visibility. Fig. 5 shows representative images of tail vein detection, needle alignment, and injection outcomes. During the injection process, the AI algorithm precise positioned

the robotic arm by successfully recognizing the trajectory of the lateral tail vein and needle. Successful injections were characterized by uniform intravascular flow of Evans blue dye along the vein (white arrow in Fig. 5a), whereas failed attempts showed local extravasation or discontinuous dye distribution. The success of the intravenous administration was visually verified by observing the systemic distribution of Evans blue, indicated by blue coloration in peripheral areas such as the ears, nose, and paws (red circles in Fig. 5b). AIIS achieved an overall injection success rate of 96% (96/100 trials) in BALB/c mice, 90% (90/100 trials) in C57BL/6 mice, and 90% (54/60 trials) in ICR mice despite the lower tail contrast of the latter under visible light. Therefore, the vision-based learning model (DeepLabv3+) maintains robust performance across different skin pigmentation backgrounds.

PK Study in Mice

The PK profile of caffeine after automated IV administration via physical AI-based AIIS was evaluated in mice across three dose groups (1, 5, and 10 mg/kg, n = 3 per group). No abnormal behavior, tail necrosis, or mortality was observed during or after dosing in any group.

Plasma samples were collected at predetermined time points (0.25, 0.5, 1, 2, 4, and 8 h) and analyzed by LC–MS/MS. The resulting plasma concentration-time curves and derived PK parameters are presented in Fig. 6 and Table 1, respectively. The plasma concentration of caffeine declined monoexponentially after intravenous dosing, and AUC_{inf} increased proportionally with the administered dose, ranging from 389.04 ± 71.45 ng·h/mL at 1 mg/kg to 6035.06 ± 1774.34 ng·h/mL at 10 mg/kg. The $t_{1/2}$ remained consistent among groups with values of 0.56 ± 0.10 h, 0.52 ± 0.12 h, and 0.59 ± 0.02 h for 1, 5, and 10 mg/kg, respectively. Although CL decreased with increasing dose (2636.50 ± 539.66 mL/h/kg at 1 mg/kg to 1756.26 ± 513.88 mL/h/kg at 10 mg/kg), the difference was not statistically significant, indicating no clear dose-dependent change in systemic clearance. Similarly, V_d showed a decreasing tendency from 2064.80 ± 25.40 mL/kg to 1496.78 ± 487.03 mL/kg, but without consistent statistical support across groups. The PK parameters exhibited low variability,

and SD values remained within approximately 30% of the mean, which further supported the consistency and reliability of the system.

DISCUSSION

The present study demonstrates that AIIS enables precise, reproducible, and ethically refined intravenous administration in mice by integrating perception, reasoning, and actuation into a closed-loop feedback framework. The combination of a vision-based deep-learning model (DeepLabv3+), robotic control, optimized optical illumination, and pressure sensing facilitated exceptionally high injection success rates of 96%, 90%, and 90% in BALB/c, C57BL/6 and ICR mice, respectively, regardless of variations in tail pigmentation or vein contrast. These findings indicate that AIIS overcomes the dependence on operator skills and environmental conditions.

Previous studies used image guidance and pressure-based confirmation to automate murine tail vascular access. Chang et al. introduced an automated mouse tail vascular access system that combined vision-based vein/needle detection with pressure feedback to facilitate vascular cannulation in anesthetized mice[6]. Similarly, Fromholtz et al. reported an image-guided robotic device that assisted tail vein cannulation by estimating the vessel location from a visual input[7]. Recent approaches have examined stereo vision and 3D image reconstruction to guide robotic needle positioning[9]. While these systems illustrate the feasibility of machine-assisted vascular access, they primarily focus on discrete subsystems of automation and lack a fully integrated closed-loop framework that continuously adapts to biological variability. In contrast, AIIS incorporates a physical AI paradigm by tightly integrating perception (DeepLabv3+-based segmentation), decision logic (alignment thresholding and retry gating), and actuation (robotic insertion and withdrawal) with physiological confirmation via pressure feedback. This holistic integration standardizes optical conditions through wavelength-optimized illumination (525–550 nm) and synchronizes multimodal sensing with robotic motion control, thereby reducing inter-animal and inter-operator variability more effectively than previous systems. This embodied feedback loop, demonstrates the potential of physical AI for

adaptive interactions with living systems.

The robust performance of the vision module (mIoU accuracy of 93.2% across multiple mouse strains) reflected the effective capture of multiscale feature representations via DeepLabv3+'s atrous spatial pyramid pooling and encoder–decoder architecture. The latency per frame (< 0.15 s) further ensured alignment fidelity under dynamic shifts in tail posture or illumination. This rapid, multi-view recognition provided reliable inputs for the robotic alignment logic, which iteratively corrected offset errors exceeding ±0.5 mm parameters that were selected based on empirical evaluation of vein diameter and injection tolerances. Simultaneously, the pressure feedback module provided an objective physiological signal to confirm intravascular entry. Characteristic pressure elevation above the 4–7 mmHg threshold upon venous penetration, followed by stable infusion and a gradual return to baseline, was consistently observed across strains. By incorporating this signal into the actuation decision path, the system mitigated the risks associated with false-positive visual alignments and reduced unnecessary tissue trauma, thereby supporting efforts to improve animal welfare and experimental reliability. The quantitative analysis of robotic motion revealed that positional deviations remained within ±0.2 mm along all spatial axes across repeated trials. Owing to the approximate diameter of murine lateral tail veins (approximately 0.3–0.6 mm), such precision ensures reliable intravascular access without repeated adjustments or manual intervention. By combining consistent pressure and vision feedback, the motion control framework of the AIIS supported smooth and repeatable injection profiles suitable for downstream applications requiring high dosing consistency.

As a well-characterized probe compound in rodents, caffeine exhibits rapid systemic elimination and shorter half-life in mice than in humans. It exhibits a monoexponential decline following intravenous or intraperitoneal administration, with $t_{1/2}$ typically below 1 h and relatively high systemic clearance, reflecting efficient hepatic metabolism in mice[16,17]. In the present study, intravenous administration of caffeine using AIIS yielded elimination half-lives of 0.52–0.59 h, which are consistent with previously reported values in mice, indicating that the observed PK profiles are physiologically consistent. Although detailed dose-dependent intravenous PK analyses of caffeine in

mice are limited, the overall findings are consistent with its rapid metabolic disposition and extensive tissue distribution. Furthermore, the relatively low variability in PK parameters (typically within 30% of the mean) supports the precision and reproducibility of the AIIS platform, highlighting its suitability for reliable in vivo PK studies.

Despite these promising results, the limitations of this study warrant further discussion. First, the PK study employed a relatively small sample size (n = 3 per group), which could have limited the statistical power and generalizability of the PK parameters. Larger cohort studies with additional compounds exhibiting a broader range of physicochemical properties are necessary to generalize the AIIS performance across diverse pharmacologies. Second, although tail vein injections are common in rodent studies, other routes, such as jugular access, were not evaluated and may require further system adaptation. Third, optimal pressure thresholds and segmentation parameters were determined empirically; although they performed well in this context, the robustness of these settings across broader biological and procedural variations (such as age and disease state) must be assessed. Additionally, although LED wavelength optimization improved vein contrast and model robustness, changes in ambient lighting or animal pigmentation extremes beyond those studied may affect image quality. Finally, the long-term sensor calibration drift and mechanical wear of the robotic components were not systematically characterized, highlighting the need for preventive maintenance protocols and real-time diagnostic indicators in future iterations.

Collectively, this study shows that the physical AI-based AIIS can transform operator-dependent tail vein injection into a standardized and adaptive closed-loop procedure by coupling real-time perception, decision-making, robotic actuation, and pressure-based physiological feedback. By achieving high injection success rates across mouse strains with different tail pigmentations, maintaining submillimeter positioning accuracy, and generating caffeine pharmacokinetic profiles consistent with established mouse caffeine pharmacokinetics, AIIS supports accurate and reproducible dosing for quantitative preclinical studies. These findings demonstrate how physical AI can bridge

robotic automation and the inherent variability of biological systems, providing a scalable platform for standardized preclinical drug administration and PK evaluation.

MATERIALS AND METHODS

Animals

All experiments on animals complied with the institutional guidelines for the care and use of laboratory animals and were approved by the Institutional Animal Care and Use Committees (IACUCs) of the Plasbio Research Institute (Approval No. PLASBIO-2024-001) and the Korea Research Institute of Bioscience and Biotechnology (KRIBB, Approval No. KRIBB-AEC-24008). Male and female BALB/c, C57BL/6, and ICR mice were obtained from Koatech (Pyeongtaek, Republic of Korea) and housed under controlled environmental conditions (temperature 22 ± 2°C, humidity 50 ± 10%, 12 h light/dark cycle) with free access to standard laboratory chow and water.

Before intravenous injection, the mice were anesthetized using isoflurane inhalation delivered through a custom-built anesthesia system integrated with the AIIS setup. Induction was achieved with 5% isoflurane at a flow rate of 400 mL/min, and anesthesia was maintained with 2%–3% isoflurane at 200 mL/min via a mask throughout the injection process. The animals were placed on a smart injection bed equipped with a temperature-controlled heating pad (maintained at 37 °C), and the tail was immobilized in a magnetic restrainer to ensure alignment stability and minimize motion artifacts during imaging and needle insertion (Fig. 7). For system performance evaluation, 87 mice were used: BALB/c (n = 38; 14 males, 24 females), C57BL/6 (n = 19; 12 males, 7 females), and ICR (n = 30; 9 males, 21 females) at the age of 5 weeks. Automated intravenous injections of saline or 8% Evans blue dye were administered. For the PK study, nine ICR mice (n = 9; males) aged 7 weeks were used.

AIIS System Overview

A physical AI-based AIIS was developed to autonomously perform intravenous administration in mice by integrating multiple hardware and software modules. The system comprised five main

components: a collaborative robotic arm, a pressure sensing module, a dual camera vision unit, a tail restraining and smart injection bed, and an inhalation anesthesia device (Fig. 7). All the components were mounted on a modular base to allow precise alignment and stable operation during automated injection.

(1) Robotic arm: A six-axis collaborative robot (model: CR series, Plasbio, Republic of Korea) was used to control needle positioning and insertion with submillimeter precision. Arm movement was governed by custom motion control software synchronized with the vision system and pressure feedback loop. The end-effector of the robot held a syringe injection unit connected to a pressure sensor and syringe pump.

(2) Pressure sensor module: A piezoresistive pressure sensor was installed between the syringe and needle via a three-way connector to monitor the real-time pressure changes during the injection process, provide feedback to verify successful intravascular entry (≥ 4–7 mmHg pressure threshold), and detect potential leakage or blockage.

(3) Dual-camera vision unit: The AIIS incorporated a dual-camera vision system comprising top-view and side-view CMOS cameras (1920 × 1080 pixels, 30 fps) for real-time tail vein detection. A dual light-emitting diode (LED) illumination system (top and bottom) provided uniform lighting, with the wavelength optimized at 525–550 nm to enhance vein visibility. The tail of each mouse was fixed in a custom three-dimensional (3D)-printed restrainer to maintain a stable imaging field. The cameras were mounted on adjustable rails for fine positional calibration. The vision data were processed in real time using a DeepLabv3+ convolutional neural network (CNN) model that segmented the tail vein and needle trajectory for accurate alignment.

(4) Tail restraining and smart injection bed: The mouse was positioned on a smart injection bed equipped with a magnetic tail restrainer to maintain consistent posture and imaging conditions. Additionally, the bed featured integrated heating control and fixation channels to stabilize the tail during imaging and injection. This configuration minimized movement artifacts and

improved reproducibility between trials.

(5) Inhalation anesthesia device: A custom-designed inhalation anesthesia system was connected to the injection bed to maintain animal sedation during the procedure. The device delivered isoflurane at controlled concentrations via a closed circuit, ensuring consistent anesthesia levels throughout the automated injection process.

All the hardware modules of the AIIS, including the robotic arm, syringe pump, dual-camera vision unit, and pressure sensor, were connected to a central robot control box that communicated with a workstation via the TCP/IP protocol. The PC served as the central processing unit and integrated hardware control and software decision-making functions. The control software, developed in Python 3.10, within a Robot Operating System based framework, synchronized visual recognition, robotic motion, and pressure feedback in real time. To achieve seamless data transfer between the perception and actuation layers, a graphical user interface (GUI) was implemented using OpenCV for image acquisition and PyTorch for model inference. The sensor and actuator signals were processed through the robot control box to ensure low-latency communication and precise synchronization across the modules. Together, these integrated hardware and software subsystems established the physical and computational foundation of the AIIS, thereby enabling precise, reproducible, and fully automated IV injections with minimal human intervention.

Algorithmic Workflow

The overall operational algorithm of AIIS consists of the following sequential steps (Fig. 8): (1) Initialization: The user mounts the syringe and verifies system readiness via the GUI. (2) Detection: Cameras capture tail images and the CNN model performs vein segmentation. (3) Alignment check: If alignment is not achieved, robotic microadjustments are executed. (4) Insertion: The robot arm inserts a needle along the predicted vein trajectory. (5) Pressure monitoring: Real-time pressure feedback is

analyzed to confirm the venous entry. (6) Infusion: The syringe pump administers the preset volume (e.g., 50 μL of solution). (7) Result logging: The system automatically stores all image, pressure, and positional data for post-analysis. This closed-loop framework embodies the physical AI principle, which continuously links perception (vision), cognition (AI-based decision), and actuation (robotic motion) to adaptively control biological interactions.

Illumination Optimization for Vision-Based Vein Recognition

To establish reliable imaging conditions for vision-based tail vein recognition, preliminary illumination optimization experiments were conducted using multiple LED wavelengths, including blue, green, yellow, red, and white LED light, and natural ambient light. Tail images were acquired from BALB/c, C57BL/6, and ICR mice using a custom imaging module with a fixed camera geometry. The gray-scale intensity difference (ΔGray value) was calculated to select the optimal LED light by estimating the absolute difference between the mean gray-scale intensities of the vein region and surrounding tissue, as measured from line intensity profiles perpendicular to the lateral tail vein. Based on this optimization procedure, green LED illumination (525–550 nm) was selected and used exclusively for all subsequent image acquisitions, including model training and real-time operations.

Vision-Based Tail Vein Recognition Using Deep Learning

The vision module for tail vein recognition was implemented using a semantic segmentation framework based on DeepLabv3+ architecture. The input images of the mouse tail were acquired under fixed green LED illumination and provided to the network as three-channel red–green–blue color images. Both the top and side views were processed to support robust spatial localization of the tail vein and injection needle (Fig. 1). The segmentation network followed an encoder-decoder structure. In the encoder, a deep CNN extracted hierarchical feature representations from the input images. Multiscale contextual information was captured by employing atrous (dilated) convolutions with multiple dilation rates (6, 12, and 18) within an atrous spatial pyramid pooling (ASPP) module, together with 1×1 convolution and image-level pooling. These parallel feature maps were

concatenated and projected through a 1×1 convolution layer to generate high-level feature representations. The decoder module progressively upsampled the encoded feature maps to recover the spatial resolution. Low-level features from earlier layers were concatenated with the upsampled high-level features to refine the boundary information. Subsequent convolution and upsampling operations produced pixel-level segmentation outputs at the original image resolution.

The network generated real-time segmentation masks for the lateral tail vein and needle tip, which were assigned to separate output channels. The segmentation results were overlaid on the live camera feed via a GUI and used to compute the positional offset between the detected vein centerline and needle tip. If the offset exceeded a predefined threshold of ±0.5 mm, corrective movements were issued to the robotic manipulator. This recognition and adjustment loop was executed within approximately 150 ms/cycle, enabling real-time closed-loop positional alignment during automated intravascular injection.

Pressure-Based Feedback Control

A miniature piezoresistive pressure sensor (range: 0–50 mmHg; resolution: 0.1 mmHg) was mounted inside the syringe needle hub to monitor the pressure changes during insertion and infusion. The pressure profiles were continuously sampled at 100 Hz. When the needle successfully entered the tail vein, the pressure increases (> 4–7 mmHg), followed by a transient drop, confirming intravascular access. This feedback signal was incorporated into the decision logic (Fig. 8). The system proceeded to the infusion step only when the pressure exceeded a preset threshold (4 mmHg). If the pressure pattern was not recognized within 5 s, the system automatically retracted the needle and repeated the alignment process.

PK Study using Physical AI-based AIIS

For pharmacokinetic (PK) studies, caffeine was administered intravenously at doses of 1, 5, and 10 mg/kg (n = 3 per group), prepared in 0.9% saline at a dose of 5 mL/kg, to mice using physical AI-

based AIIS. Blood samples (approximately 60 μL) were collected from the femoral vein at 0.25, 0.5, 1, 2, 4, and 8 h post-administration into heparinized tubes, followed by centrifugation at 12,000 rpm for 3 min at 4 °C. Supernatant plasma was separated and stored at −20 °C until liquid chromatography-tandem mass spectrometry (LC-MS/MS) analysis. All animals were continuously monitored during and after the procedure to evaluate for abnormal behavior, tail necrosis, or mortality.

To quantify caffeine, 20 μL of mouse plasma was mixed with 80 μL of a 10 ng/mL carbamazepine solution in acetonitrile, used as an internal standard. The mixture was vortexed for 30 s and centrifuged at 13,000 rpm for 10 min at 4 °C to precipitate plasma proteins. After centrifugation, 70 μL of the supernatant was collected and injected into the LC-MS/MS system for analysis. Quantification was performed using a LC-MS/MS system equipped with an Agilent 1260 HPLC system (Agilent Technologies, Santa Clara, CA, USA) and API 3200 QTRAP mass spectrometer (Applied Biosystems, Foster City, CA, USA). The mass spectrometer was operated in the multiple reaction monitoring mode with positive electrospray ionization. Chromatographic separation was achieved using an XTERRA MS C18 column (3.5 μm, 2.1 × 50 mm; Waters, Milford, MA, USA) with gradient elution. The mobile phase consisted of 0.3% formic acid in water (solvent A) and 0.3% formic acid in acetonitrile (solvent B) and the flow rate was 300 μL/min. Gradient elution was performed with A:B ratios of 95:5 (v/v) from 0 to 0.5 min and then 5:95 (v/v) for 2.0 min, and returned to the initial composition at 3.5 min, which was maintained for equilibration for 5 min. The retention times of caffeine and carbamazepine were 2.75 min and 3.16 min, respectively. The mass-to-charge ratio (m/z) transitions monitored were m/z 195.2 → 138.1 and m/z 237.2 → 194.2 for caffeine and carbamazepine, respectively.

PK Analysis

The PK parameters were calculated using non-compartmental analysis (NCA) of plasma concentration-time data. Essential parameters, such as the area under the plasma concentration-time curve to the last measurable point (AUC_{last}), area under the plasma concentration-time curve

extrapolated to infinity (AUC_{inf}), elimination half-life ($t_{1/2}$), volume of distribution (V_d), and clearance (CL) were calculated using Phoenix WinNonlin software (Version 8.4, Certara, Princeton, NJ, USA). The AUC was calculated using the linear trapezoidal-linear interpolation rule. The PK parameters were expressed as the mean ± standard deviation (SD).

Statistical Analysis

NCA was performed using single-species (mouse) data to calculate the PK parameters. Statistical analysis was performed using a one-way analysis of variance (ANOVA) to compare the PK parameters between the different normalized dose groups (1, 5, and 10 mg/kg). Statistical significance was set at $p < 0.05$.

Author Contributions: Y.-J.C: Conceptualization, methodology, investigation, data curation, visualization, and writing of the original draft. **J.-Y.L.:** Conceptualization, methodology, investigation, data curation, visualization, and writing of the original draft. **H.-C.J:** Conceptualization, methodology, and writing of the original draft. **R.-W.K:** Conceptualization, methodology, investigation, and writing of the original draft. **H.-J.G.:** Methodology, investigation, and writing of the original draft. **K.-S.K.:** Methodology, investigation, and writing of the original draft. **K.-H.N:** Conceptualization, methodology, and writing of the original draft. **S.-G.P.:** Conceptualization, methodology, visualization, writing the original draft, supervision, project administration, and funding acquisition. **K.-R.L.:** Conceptualization, methodology, visualization, writing the original draft, supervision, project administration, and funding acquisition.

Funding Information

This research was supported by the Institute of Civil Military Technology Cooperation funded by the Defense Acquisition Program Administration and the Ministry of Trade, Industry, and Energy of the Korean Government (No. 23-CM-BR-09), and by the Korea Research Institute of Bioscience and

Biotechnology (KRIBB) Research Initiative Program grant KGM1312612, "Establishment and support of infrastructure for the utilization of laboratory animal resources".

Data availability

The datasets generated and/or analysed during the current study are available from the corresponding author upon reasonable request.

Code availability

The trained model weights and custom control software are available from the corresponding author on reasonable request.

Competing interests

S.G.P. and R.-W.K. are employees of PLASBIO Inc., which developed and manufactures the robotic injection system (AIIS) evaluated in this study. The other authors declare no competing interests.

References

1. Yan, S.-K. et al. 'Omics' in pharmaceutical research: overview, applications, challenges, and future perspectives. Chin. J. Nat. Med. 13, 3–21 (2015).

2. Vitorino, R. Transforming clinical research: the power of high-throughput omics integration. Proteomes 12, 25 (2024).

3. Aldewachi, H., Al-Zidan, R. N., Conner, M. T. & Salman, M. M. High-throughput screening platforms in the discovery of novel drugs for neurodegenerative diseases. Bioengineering (Basel) 8, 30 (2021).

4. Dueñas, M. E. et al. Advances in high-throughput mass spectrometry in drug discovery. EMBO

Mol. Med. 15, e14850 (2023).

5. Ashiwaju, B. I., Orikpete, O. F. & Uzougbo, C. G. The intersection of artificial intelligence and big data in drug discovery: a review of current trends and future implications. Matrix Sci. Pharma 7, 36–42 (2023).

6. Chang, Y.-C. et al. An automated mouse tail vascular access system by vision and pressure feedback. IEEE ASME Trans. Mechatron. 20, 1616–1623 (2015).

7. Fromholtz, A. et al. Design and evaluation of a robotic device for automated tail vein cannulations in rodent models. J. Med. Device 11, 041008 (2017).

8. Turner, P. V., Brabb, T., Pekow, C. & Vasbinder, M. A. Administration of substances to laboratory animals: routes of administration and factors to consider. J. Am. Assoc. Lab. Anim. Sci. 50, 600–613 (2011).

9. Ko, T. et al. Development of a stereo-vision based high-throughput robotic system for mouse tail vein injection. In 2022 IEEE International Conference on Robotics and Automation (ICRA) 1777–1783 (IEEE, 2022).

10. Bernardes, M. C. et al. In vivo feasibility study: evaluating autonomous data-driven robotic needle trajectory correction in MRI-guided transperineal procedures. IEEE Robot. Autom. Lett. 9, 8975–8982 (2024).

11. Häse, F., Roch, L. M. & Aspuru-Guzik, A. Next-generation experimentation with self-driving laboratories. Trends Chem. 1, 282–291 (2019).

12. Coley, C. W. et al. A robotic platform for flow synthesis of organic compounds informed by AI planning. Science 365, eaax1566 (2019).

13. Thakur, A. et al. Physical artificial intelligence for powering the next revolution in robotics. J. Comput. Inf. Sci. Eng. 25, 120809 (2025).

14. Li, H. et al. Digital twin and AI-driven robotic embodied control system: a novel adaptive learning and decision optimization method. Robot. Comput. Integr. Manuf. 98, 103138 (2026).

15. Kiew, C. Y. K., Shah, A., Hadjiandreou, M. & Pafitanis, G. Artificial intelligence in microsurgery and supermicrosurgery training within plastic surgery: a systematic review. JPRAS Open 46, 154–168 (2025).

16. Hartmann, M. & Czok, G. Pharmacokinetics of caffeine in mice and its modification by ethanol. Z. Ernahrungswiss. 19, 215–227 (1980).

17. SC, Y. & Muralidhara. Beneficial role of coffee and caffeine in neurodegenerative diseases: a minireview. AIMS Public Health 3, 407–422 (2016).

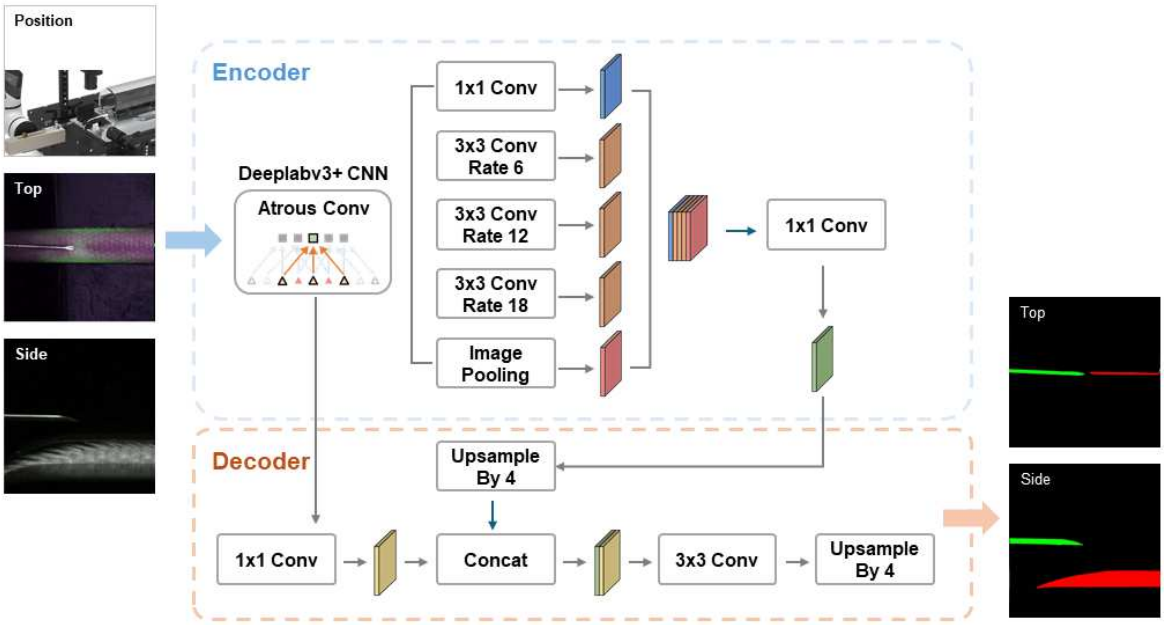

Figure 1. Schematic of the DeepLabv3+–based encoder–decoder network used for tail vein recognition. Top- and side-view images are processed by an encoder with atrous spatial pyramid pooling (ASPP) to extract multi-scale features, followed by a decoder that upsamples feature maps to generate pixel-level segmentation of the tail vein (red line) and needle tip (green line).

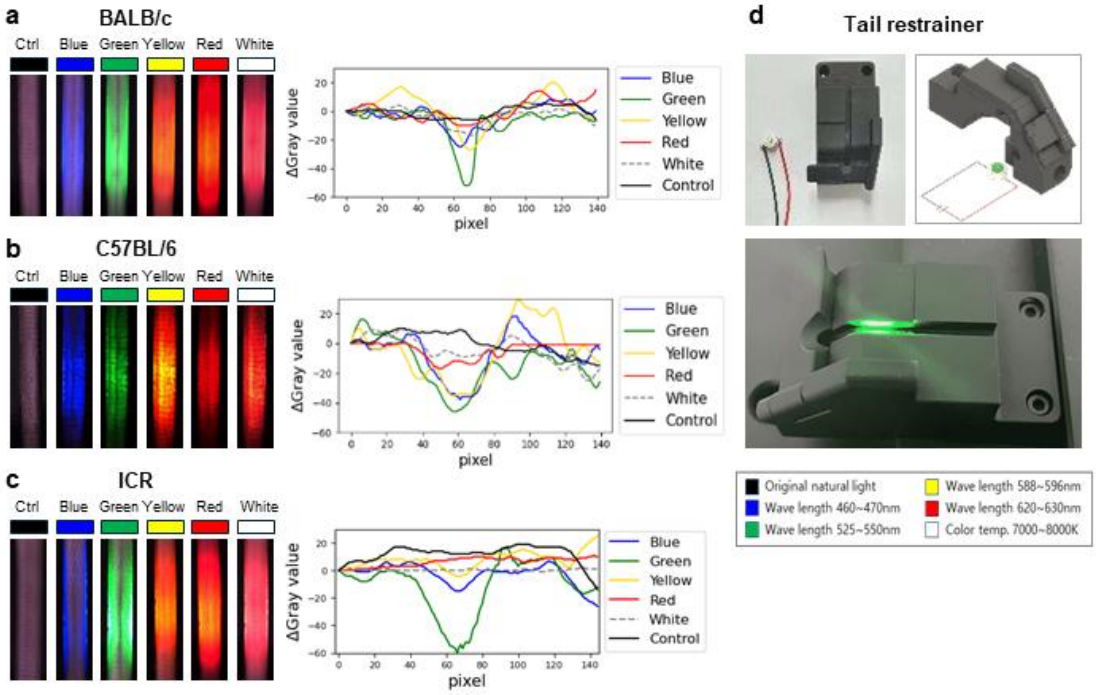

Figure 2. Optimization of LED illumination for tail vein visualization. (a-c) Representative tail images and corresponding gray-scale intensity difference (ΔGray) profiles measured across the lateral tail vein in BALB/c (a), C57BL/6 (b), and ICR mice (c) under different LED illumination wavelengths. (d) Photographs and schematics of the custom-designed LED illumination module and tail restrainer, including a magnified view of the tail positioned within the device under green LED lighting.

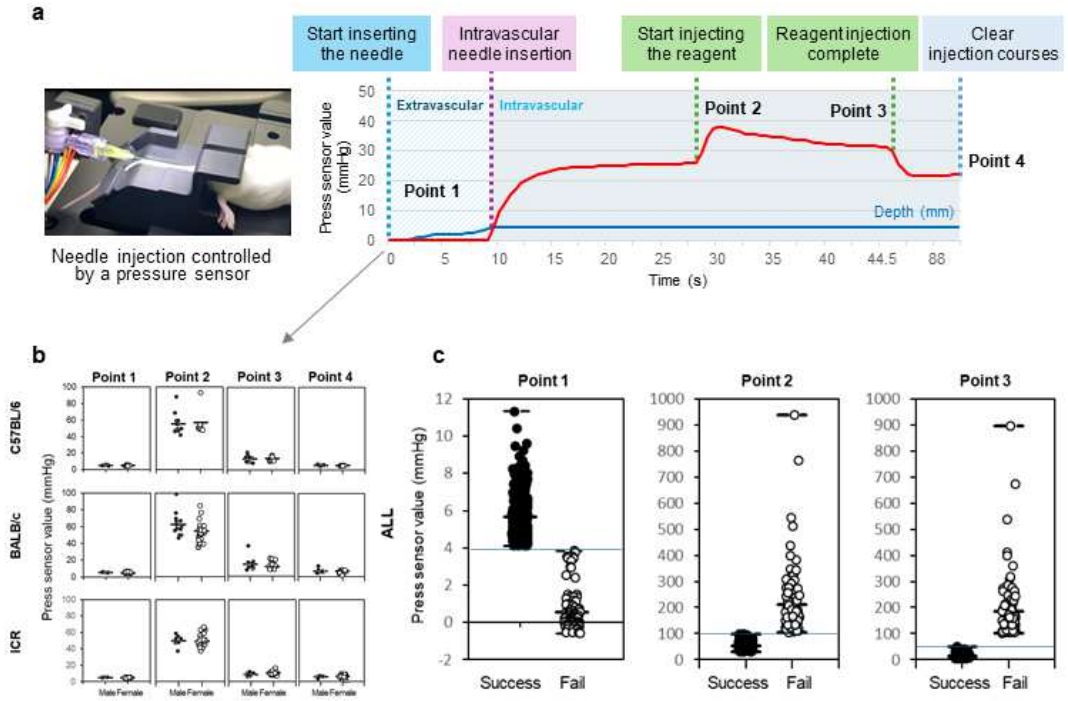

Figure 3. Real-time pressure-based feedback during automated tail vein injection. (a) Representative image of the automated tail vein injection procedure performed by the AIIS and pressure–depth profile recorded during a successful intravascular injection. (b) Scatter plots of pressure values recorded at Points 1, 2, 3, and 4 during successful intravascular injections in each mouse strain, demonstrating consistent pressure elevations above the predefined threshold. The closed and open circles present male and female mice, respectively. (c) Scatter plots of pressure values recorded at Point 2 during successful (closed circles) and unsuccessful (extravascular) insertions (open circles).

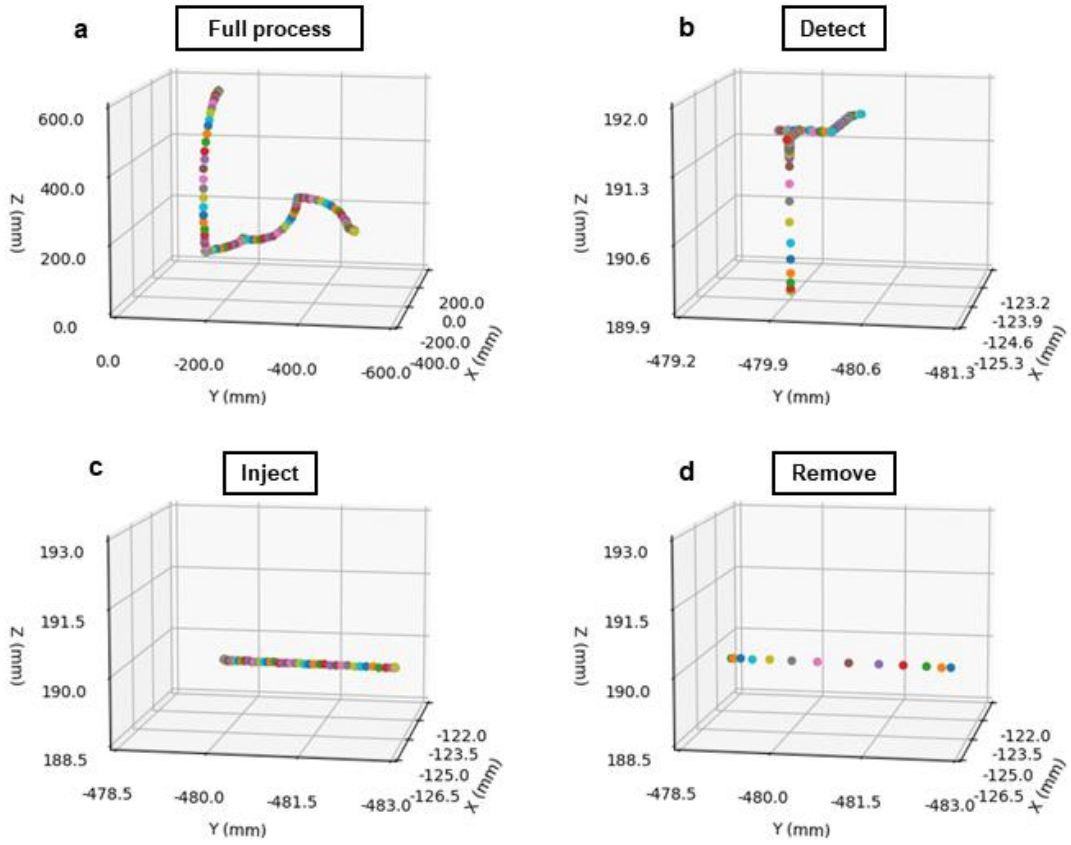

Figure 4. Three-dimensional robotic motion trajectories during automated injection. (a) Full robotic trajectory of the automated injection process. (b) Detection phase showing needle approach and alignment. (c) Injection phase showing linear motion at constant depth. (d) Removal phase showing controlled needle retraction.

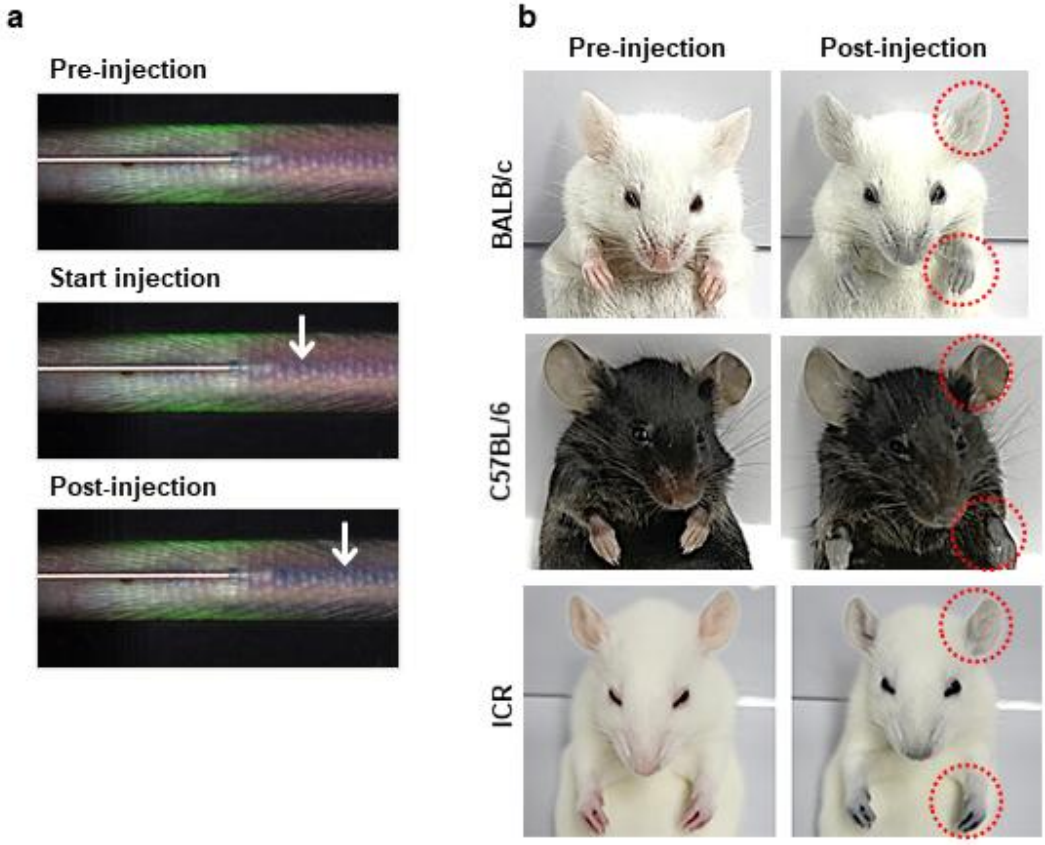

Figure 5. Visual evaluation of automated tail vein injection performance. (a) Representative images showing tail vein detection, needle alignment, and intravascular flow of Evans blue dye along the tail vein during automated injection. The white arrows indicate uniform dye distribution within the vein. (b) Representative images showing systemic distribution of Evans blue dye in peripheral regions (ears and paws, dashed circles) following successful intravenous injection in BALB/c, C57BL/6, and ICR mice.

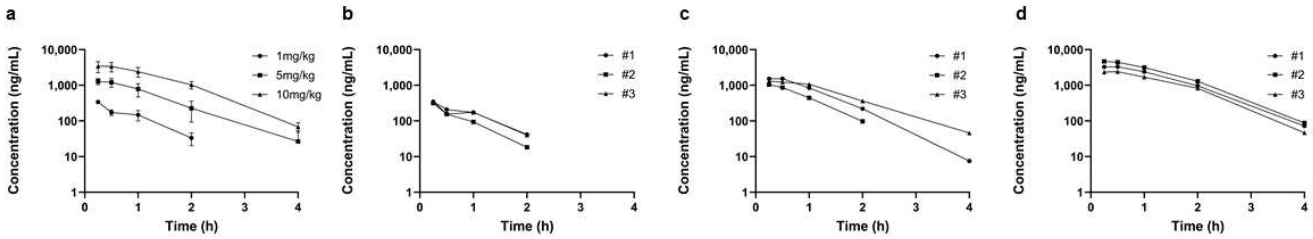

Figure 6. PK study of caffeine in mice using Physical AI-based AIIS. (a) Mean plasma concentration-time profiles (± SD) of caffeine after single intravenous administration to mice. (b-d) Individual plasma concentration-time profiles of caffeine after a single intravenous administration of doses of (b) 1, (c) 5, and (d) 10 mg/kg to mice.

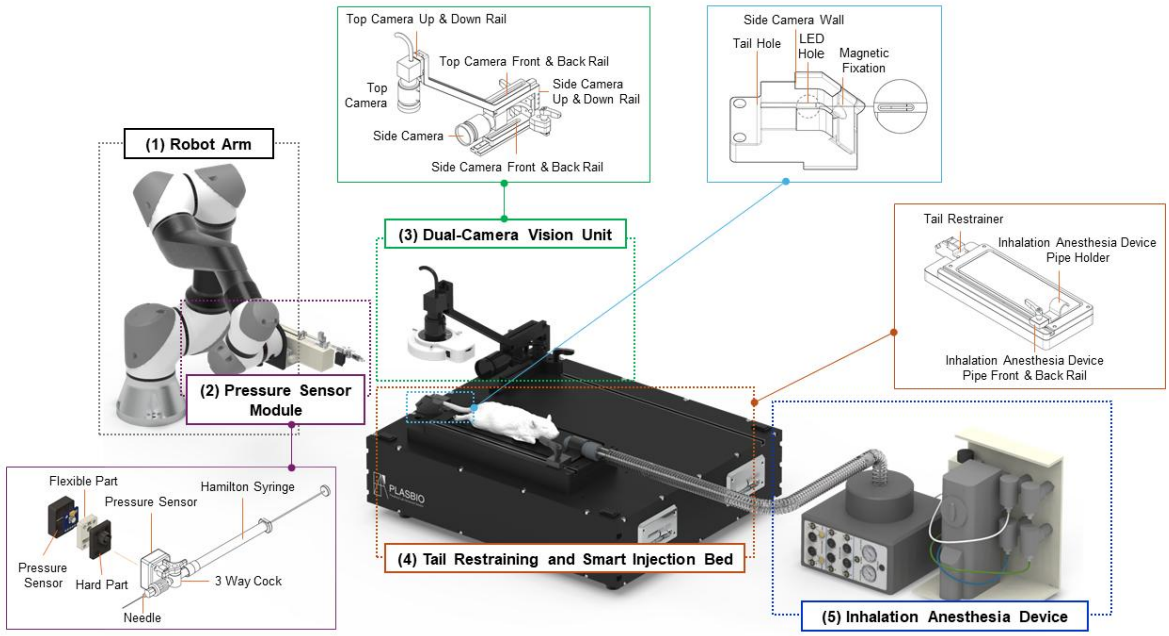

Figure 7. Schematic and hardware configuration of the Physical AIIS developed for autonomous tail vein intravenous injection in mice. The system consists of five integrated modules: (1) a six-axis collaborative robotic arm; (2) a pressure sensor module installed between the syringe and needle; (3) a dual-camera vision unit (top and side views) combined with wavelength-optimized green LED illumination; (4) a tail restraining and smart injection bed equipped with temperature control and magnetic fixation; and (5) an inhalation anesthesia device for maintaining controlled isoflurane anesthesia.

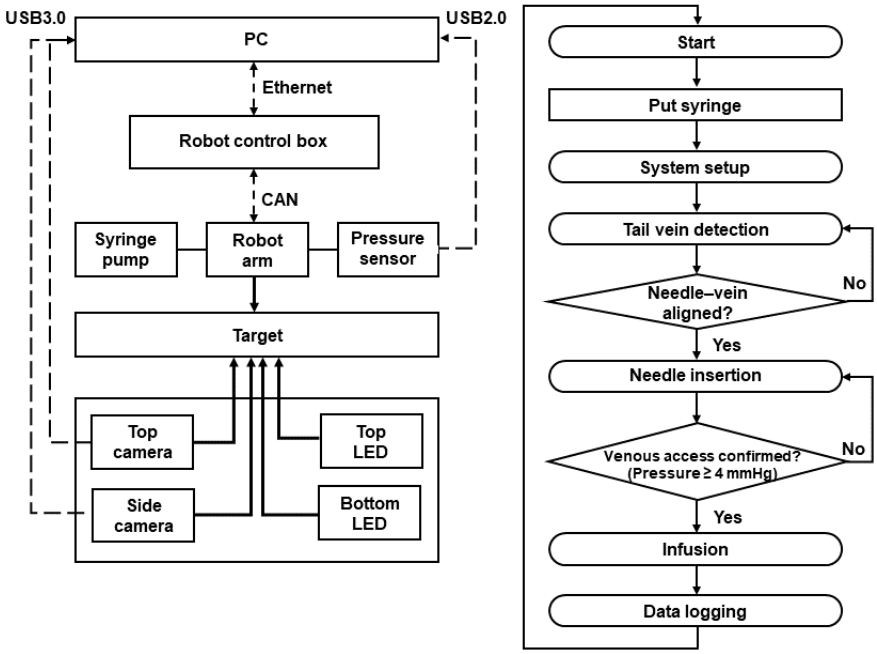

Figure 8. System architecture and closed-loop workflow of the AIIS. Block diagram of the Physical AIIS. The system integrates a PC, robot control box, robotic arm, syringe pump, pressure sensor, and dual-camera vision unit with LED illumination. Real-time image processing guides robotic alignment, while pressure feedback (>4 mmHg) confirms intravascular access. The closed-loop workflow enables automated detection, alignment, needle insertion, infusion, and data logging.

Table 1. PK Parameters of Caffeine in Mice Following Intravenous Administration at Doses of 1, 5, and 10 mg/kg using Physical AI-based AIIS

Dose (mg/kg)	1 mg/kg	5 mg/kg	10 mg/kg
AUC_{last} (ng·h/mL)	361.13 ± 57.51	1860 ± 651.12	5977.36 ± 1759.39
AUC_{inf} (ng·h/mL)	389.04 ± 71.45	1898.61 ± 631.22	6035.06 ± 1774.34
CL (mL/h/kg)	2636.50 ± 539.66	2887.79 ± 1153.39	1756.26 ± 513.88
V_d (mL/kg)	2064.80 ± 25.40	2119.45 ± 702.86	1496.78 ± 487.03
$T_{1/2}$ (h)	0.56 ± 0.10	0.52 ± 0.12	0.59 ± 0.02

ANOVA did not indicate statistically significant differences among groups.

Supplementary Files

This is a list of supplementary files associated with this preprint. Click to download.

- reportingsummaryLananimal.pdf